Networks and Heterogeneous Media

https://www.aimspress.com/journal/nhm

NHM, 21(2): 426–445.
DOI: 10.3934/nhm.2026020
Received: 24 January 2026
Revised: 03 March 2026
Accepted: 16 March 2026
Published: 25 March 2026

Research article

Analysis and simulation of the effect of fractional parameters on dynamic behavior for a fractional-in-time three-species reaction-diffusion model

Hao Lu Zhang [1,2,*], **Xiao Yu Li**[3,*] **and Zhi Yuan Li**[3,*]

[1] College of Civil Engineering, Inner Mongolia University of Technology, Hohhot 010051, China

[2] Production and Operation Center, CCCC Comprehensive Planning and Design Institute Co. Ltd., Beijing 100024, China

[3] College of Intelligent Science and Technology, Inner Mongolia University of Technology, Hohhot 010080, China

* **Correspondence:** Email: 18586053173@163.com, fish_li82@163.com, lizhiyuan2064@126.com.

Abstract: This paper investigates a three-species reaction-diffusion model with fractional-order derivatives and proposes an innovative numerical method for its simulation. The method integrates an optimized Grünwald-Letnikov discretization scheme, enhanced by a short-memory principle, with a high-order accurate nine-point compact difference scheme, enabling an efficient and stable solution of fractional operators. Rigorous convergence and stability analyses confirm the theoretical reliability of the algorithm. Through stability and Turing bifurcation analyses, the study systematically reveals the regulatory mechanism of the fractional-order exponent on the dynamic behavior of the system. The numerical results demonstrate that the present method accurately captures the effect of fractional derivatives on the formation process of spatial patterns.

Keywords: a numerical method; fractional reaction-diffusion; pattern formation; short-memory principle; stability analysis

1. Introduction

Spatiotemporal pattern formation in ecosystems is a central theme in theoretical ecology, and is crucial to understand species coexistence, community stability, and ecosystem functioning [1, 2]. Patterns such as traveling waves, periodic oscillations, and chaotic dynamics emerge from the interplay of biological interactions, dispersal processes, and environmental heterogeneity. Reaction–diffusion models have long provided a powerful framework to investigate such phenomena, thereby revealing how local interactions scale up to macroscopic spatial structures.

Classical integer-order models assume instantaneous or exponentially fading memory in species responses. However, ecological processes often exhibit memory effects, time lags, and non-local temporal dependencies that are better captured by fractional calculus [3, 4]. Fractional derivatives incorporate memory and hereditary properties, thus allowing for more realistic representation of growth, competition, and predation dynamics across trophic levels. In particular, fractional-order reaction–diffusion systems can describe anomalous diffusion and long-range temporal correlations, which are observed in species movement, resource uptake, and population recovery [5, 6].

Recent years have witnessed significant progress in the development and analysis of fractional-order ecological models. For instance, reference [7] proposed positivity and boundedness preserving schemes for space-time fractional predator-prey models, while [8] compared pattern formations in fractional and classical reaction-diffusion systems. The works of [9] further extended the mathematical and computational studies of fractional predator-prey interactions, thereby highlighting the role of Caputo derivatives in modeling complex dynamics. The inclusion of cross-fractional diffusion and delay has been shown to induce rich spatiotemporal patterns [1], and chaotic oscillations have been extensively studied in fractional reaction-diffusion systems [10, 11].

Additionally, theoretical advances have also been made in understanding the qualitative properties of fractional systems. Reference [12] established a Liouville theorem for a class of reaction-diffusion systems with fractional diffusion, thus providing important insights into the existence and boundedness of solutions. Numerical methods to solve such systems have been actively developed, including high-precision Fourier spectral approaches [13] and novel finite difference schemes [11]. Applications have expanded to various ecological contexts, such as models with interval biological coefficients [14]. Recent studies have explored new pattern dynamics in fractional-order models, including those with Holling-type functional responses [15, 16], anti-predator behaviors [17], prey-taxis effects [18, 19], and multi-variable Oregonator models [20], the fractional-order-in-time Lengyel-Epstein reaction-diffusion system [21], and fractional phytoplankton-zooplankton ecological model [22].

In this paper, we extend the well-established Bazykin-type three-species predator–prey model to a fractional-order reaction–diffusion model. The system consists of prey u, mesopredator v, and apex predator w, with Holling type II functional responses and intraspecific competition. Unlike previous integer-order studies, we introduce the Grünwald-Letnikov fractional derivative $\partial^{\theta_i}/\partial t^{\theta_i}$ $(0 < \theta_i \leq 1)$ for each species, where θ_i controls the memory effect and dynamic rate of the corresponding trophic level. The model reads as follows

$$\begin{cases} \dfrac{\partial^{\theta_1} u}{\partial t^{\theta_1}} = D_u \nabla^2 u + u\left[\zeta(\kappa - u) - \dfrac{\alpha v}{\gamma_1 + u}\right], \\ \dfrac{\partial^{\theta_2} v}{\partial t^{\theta_2}} = D_v \nabla^2 v + \epsilon_1 v\left[\dfrac{\alpha u}{\gamma_1 + u} - \dfrac{\beta w}{\gamma_2 + v} - \eta_1 - \delta_1 v\right], \\ \dfrac{\partial^{\theta_3} w}{\partial t^{\theta_3}} = D_w \nabla^2 w + \epsilon_1 \epsilon_2 w\left[\dfrac{\beta v}{\gamma_2 + v} - \eta_2 - \delta_2 w\right], \end{cases} \tag{1.1}$$

where $0 < \theta_1, \theta_2, \theta_2 \leq 1$ denote the fractional orders, D_u, D_v, D_w are diffusion coefficients, other parameters $\zeta, \kappa, \alpha, \beta, \gamma_1, \gamma_2, \eta_1, \eta_2, \delta_1, \delta_2$ are ecological parameters, and ϵ_1, ϵ_2 represent timescale separations across trophic levels. The parameters are defined in Table 1.

Table 1. Parameters and their meanings.

Symbol	Meaning
ζ	Prey growth rate
κ	Carrying capacity
α	Predation rate (prey by intermediate predator)
γ_1	Half-saturation constant for u
β	Predation rate (intermediate by top predator)
γ_2	Half-saturation constant for v
η_1	Mortality rate of intermediate predator
η_2	Mortality rate of top predator
δ_1	Intraspecific competition of v
δ_2	Intraspecific competition of w
ϵ_1	Time scale for intermediate predator
ϵ_2	Time scale for top predator
D_u	Diffusion coefficient of prey
D_v	Diffusion coefficient of intermediate predator
D_w	Diffusion coefficient of top predator

The main contributions of this paper are as follows:

- We propose an optimized Grünwald-Letnikov fractional discretization scheme combined with a short-memory principle and a fourth-order accurate nine-point compact finite difference scheme. This hybrid approach ensures both computational efficiency and numerical stability in simulating the fractional-order reaction-diffusion system.
- We establish detailed error estimates and prove the convergence order of the numerical scheme. A stability analysis is conducted, and explicit stability conditions are derived, thus ensuring the reliability of long-term simulations.
- Through comprehensive numerical experiments, we systematically analyze how fractional orders influence the formation, evolution, and morphology of Turing patterns.

This paper is organized as follows.

In Section 2, we perform the stability analysis of the fractional-order three-species predator-prey reaction-diffusion model, including the determination of equilibrium points and the derivation of the characteristic equation for local asymptotic stability. In Section 3, we introduce the numerical scheme, which combines an optimized Grünwald-Letnikov discretization with a short-memory principle and a high-order nine-point compact finite difference method for spatial discretization. Section 4 presents the convergence and stability analysis of the proposed numerical method, providing theoretical error bounds and stability conditions. In Section 5, we conduct numerical simulations to investigate pattern formation under various fractional orders and parameter sets, illustrating the effects of memory and diffusion on spatiotemporal dynamics. Finally, in Section 6, we summarize the main findings and discuss potential directions for future research.

2. Stability analysis

To analyze the dynamics of the fractional-order system (1), we first investigate the stability of its homogeneous steady states. These equilibrium points are found by solving the temporal non-spatial counterpart of the model, which is obtained by setting the diffusion terms and the time derivatives to zero:

$$\begin{cases} u\left[\zeta(\kappa-u)-\dfrac{\alpha v}{\gamma_1+u}\right]=0, \\ \epsilon_1 v\left[\dfrac{\alpha u}{\gamma_1+u}-\dfrac{\beta w}{\gamma_2+v}-\eta_1-\delta_1 v\right]=0, \\ \epsilon_1\epsilon_2 w\left[\dfrac{\beta v}{\gamma_2+v}-\eta_2-\delta_2 w\right]=0. \end{cases} \tag{2.1}$$

Solving Eq (2.1) yields several equilibrium points of ecological interest. The trivial equilibrium is $E_0 = (0, 0, 0)$. The predator-free equilibrium, which represents a state with only prey, is $E_1 = (\kappa, 0, 0)$ and always exists. Of greater interest is the coexistence equilibrium, denoted $E_* = (u^*, v^*, w^*)$, where all three species have positive densities $(u^*, v^*, w^* > 0)$. This equilibrium is obtained by solving the following system as follows

$$\zeta(\kappa-u^*)-\frac{\alpha v^*}{\gamma_1+u^*}=0, \tag{2.2}$$

$$\frac{\alpha u^*}{\gamma_1+u^*}-\frac{\beta w^*}{\gamma_2+v^*}-\eta_1-\delta_1 v^*=0, \tag{2.3}$$

$$\frac{\beta v^*}{\gamma_2+v^*}-\eta_2-\delta_2 w^*=0. \tag{2.4}$$

From Eq (2.4), an explicit expression for the top-predator equilibrium density w^* is derived:

$$w^*=\frac{1}{\delta_2}\left(\frac{\beta v^*}{\gamma_2+v^*}-\eta_2\right). \tag{2.5}$$

A biologically meaningful coexistence equilibrium requires $\frac{\beta v^*}{\gamma_2+v^*} > \eta_2$, which means that the predation benefit for the top predator must exceed its mortality rate.

Substituting w^* into Eq (2.3) yields an equation relating u^* and v^*. Subsequently, v^* can be expressed as a function of u^* using Eq (2.2):

$$v^*=\frac{\zeta(\kappa-u^*)(\gamma_1+u^*)}{\alpha}. \tag{2.6}$$

Here, the biological feasibility condition $0 < u^* < \kappa$ must hold. A closed-form solution for u^* is generally not available, so it is typically determined numerically by substituting the expression for v^* into a modified form of Eq (2.3).

To assess the local stability of a general equilibrium point $\bar{E} = (\bar{u}, \bar{v}, \bar{w})$, we analyze the system's response to small perturbations. We introduce spatially inhomogeneous perturbations in the form of plane waves: $(\tilde{u}, \tilde{v}, \tilde{w})e^{\lambda t + i\mathbf{k}\cdot\mathbf{r}}$, where λ is the temporal growth rate, $\mathbf{k}$ is the wave vector, and $k = |\mathbf{k}|$

is the wavenumber. Linearizing system (1) around $\bar{E}$ leads to the following Jacobian matrix, which incorporates both reaction kinetics and diffusion:

$$J(\bar{E}, k^2) = \begin{pmatrix} a_{11} - D_u k^2 & a_{12} & a_{13} \\ a_{21} & a_{22} - D_v k^2 & a_{23} \\ a_{31} & a_{32} & a_{33} - D_w k^2 \end{pmatrix},$$

where the matrix entries a_{ij} are the partial derivatives of the reaction terms evaluated at $\bar{E}$:

$$a_{11} = \zeta(\kappa - 2\bar{u}) - \frac{\alpha\bar{v}\gamma_1}{(\gamma_1 + \bar{u})^2}, \qquad a_{12} = -\frac{\alpha\bar{u}}{\gamma_1 + \bar{u}}, \qquad a_{13} = 0,$$

$$a_{21} = \frac{\epsilon_1\alpha\gamma_1\bar{v}}{(\gamma_1 + \bar{u})^2}, \qquad a_{22} = \epsilon_1\left(\frac{\alpha\bar{u}}{\gamma_1 + \bar{u}} - \frac{\beta\gamma_2\bar{w}}{(\gamma_2 + \bar{v})^2} - \eta_1 - 2\delta_1\bar{v}\right), \qquad a_{23} = -\frac{\epsilon_1\beta\bar{v}}{\gamma_2 + \bar{v}},$$

$$a_{31} = 0, \qquad a_{33} = \epsilon_1\epsilon_2\left(\frac{\beta\bar{v}}{\gamma_2 + \bar{v}} - \eta_2 - 2\delta_2\bar{w}\right) \qquad a_{32} = \frac{\epsilon_1\epsilon_2\beta\gamma_2\bar{w}}{(\gamma_2 + \bar{v})^2}.$$

The stability is determined by the roots λ of the characteristic equation $\det(J - \lambda I) = 0$. For a fractional-order system, this equation takes a form that accounts for the multi-valued nature of the fractional power of λ. Specifically, by substituting λ with λ^m, where m is the least common multiple of the denominators of the fractional orders θ_i, we obtain the following

$$\det\begin{pmatrix} \lambda^{m\theta_1} - (a_{11} - D_u k^2) & -a_{12} & 0 \\ -a_{21} & \lambda^{m\theta_2} - (a_{22} - D_v k^2) & -a_{23} \\ 0 & -a_{32} & \lambda^{m\theta_3} - (a_{33} - D_w k^2) \end{pmatrix} = 0. \tag{2.7}$$

Expanding the determinant in Eq (2.7) yields a fractional-order polynomial in λ as follows

$$\lambda^{m(\theta_1+\theta_2+\theta_3)} + C_1\lambda^{m(\theta_1+\theta_2)} + C_2\lambda^{m(\theta_1+\theta_3)} + C_3\lambda^{m(\theta_2+\theta_3)} + C_4\lambda^{m\theta_1} + C_5\lambda^{m\theta_2} + C_6\lambda^{m\theta_3} + C_7 = 0, \tag{2.8}$$

where the coefficients C_i are functions of a_{ij} and k^2:

$$\begin{aligned} &C_1 = -(a_{33} - D_w k^2), \qquad C_2 = -(a_{22} - D_v k^2), \qquad C_3 = -(a_{11} - D_u k^2), \\ &C_4 = (a_{22} - D_v k^2)(a_{33} - D_w k^2) - a_{23}a_{32}, \qquad C_5 = (a_{11} - D_u k^2)(a_{33} - D_w k^2), \\ &C_6 = (a_{11} - D_u k^2)(a_{22} - D_v k^2) + a_{12}a_{21}, \\ &C_7 = -(a_{11} - D_u k^2)(a_{22} - D_v k^2)(a_{33} - D_w k^2) + a_{23}a_{32}(a_{11} - D_u k^2) - a_{12}a_{21}(a_{33} - D_w k^2). \end{aligned}$$

The parameter m is defined as $m = \mathrm{lcm}(\mathrm{denom}(\theta_1), \mathrm{denom}(\theta_2), \mathrm{denom}(\theta_3))$, where $\mathrm{denom}(\theta)$ is the denominator of the rational number θ in its reduced form. For the equilibrium $\bar{E}$ to be locally asymptotically stable, all roots λ_i of the characteristic equation (2.8) must satisfy the Matignon stability criterion for commensurate fractional-order systems:

$$|\arg(\lambda_i)| > \frac{\pi}{2m} \quad \text{for all } i. \tag{2.9}$$

To facilitate the analysis, we define a stability function as follows

$$f(\theta_1, \theta_2, \theta_3, k^2) = \min_i |\arg(\lambda_i)| - \frac{\pi}{2m}. \tag{2.10}$$

The equilibrium $\bar{E}$ is locally asymptotically stable if $f(\cdot) > 0$ for all relevant $k^2 \geq 0$. This leads to two key scenarios:

- For the non-spatial system ($k = 0$), stability requires $f(\theta_1, \theta_2, \theta_3, 0) > 0$. If this holds, then the homogeneous equilibrium is stable in the absence of diffusion.
- For the spatial system, if $f(\theta_1, \theta_2, \theta_3, k^2) > 0$ for **all** $k^2 \geq 0$, then the homogeneous steady state is stable against any spatial perturbation, and no diffusion-driven instability occurs. Conversely, if there exists a range of wavenumbers k^2 for which $f(\cdot) < 0$, the homogeneous state is destabilized by diffusion, which leads to the emergence of Turing patterns.

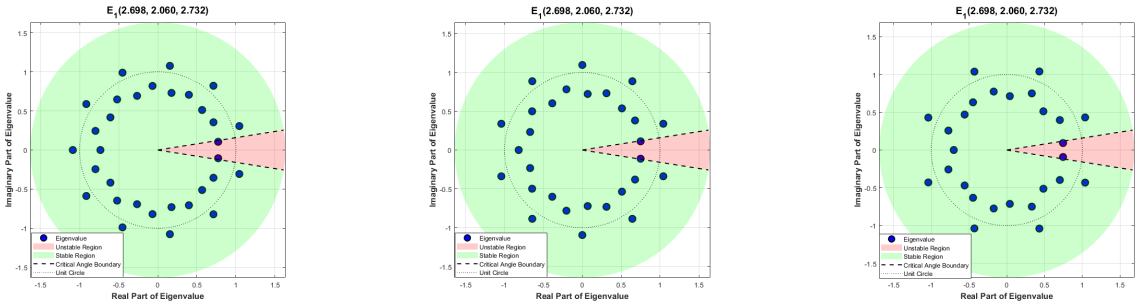

(a) $\theta_1 = 1.1, \theta_2 = 1.1, \theta_3 = 1.0$ (b) $\theta_1 = 1.0, \theta_2 = 1.0, \theta_3 = 0.9$ (c) $\theta_1 = 0.8, \theta_2 = 1.1, \theta_3 = 0.8$

Figure 1. Eigenvalue distribution of the non-spatial system ($k = 0$) for different fractional orders θ_i. All other parameters are fixed at the following $\zeta = 2.65$, $\kappa = 3.0$, $\alpha = 2.8$, $\gamma_1 = 4.5$, $\beta = 0.5$, $\gamma_2 = 1.0$, $\eta_1 = 0.5$, $\eta_2 = 0.2$, $\delta_1 = 0.05$, $\delta_2 = 0.05$, $\epsilon_1 = 0.8$, $\epsilon_2 = 0.8$. The dashed line indicates the stability boundary $|\arg(\lambda)| = \pi/(2m)$.

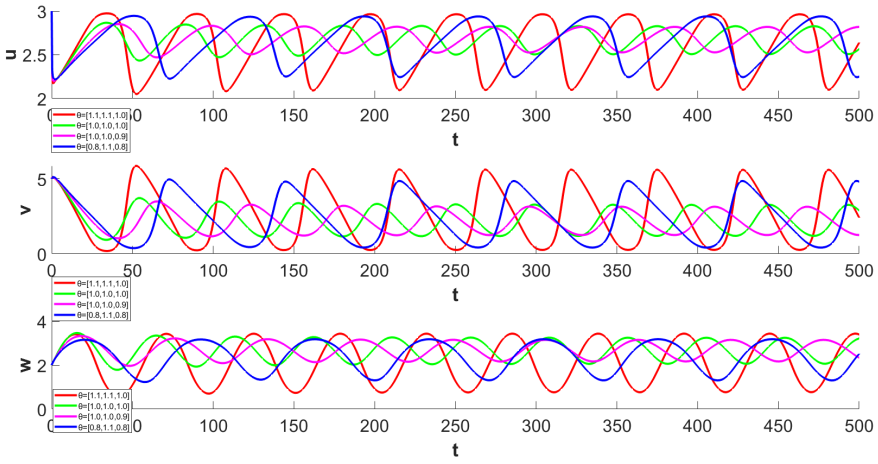

Figure 2. Time series of the three species (u, v, w) for different fractional orders, with initial conditions $x_0 = [3, 5, 2]$. Parameters are identical to those in Figure 1.

Figure 1 shows the eigenvalue distribution of the linearized system without diffusion ($k = 0$) under a baseline parameter set. The eigenvalues are plotted in the complex plane. For all tested fractional-order

combinations, the eigenvalues lie within the stable region, which satisfy $|\arg(\lambda_i)| > \pi/(2m)$. This confirms that the homogeneous equilibrium is locally asymptotically stable in the absence of spatial diffusion for this parameter set, which means that no diffusion-driven instability is expected under these conditions.

Figure 2 presents the temporal dynamics corresponding to the stable equilibrium in Figure 1. It illustrates how the memory effect, intrinsic to fractional derivatives, influences transient dynamics. As the fractional order θ decreases (e.g., from 1.0 to 0.85), the damping of oscillations becomes progressively slower, and the system exhibits a longer memory of its initial state. This is in stark contrast to the integer-order case ($\theta = 1.0$), where oscillations decay more rapidly in an exponential-like fashion.

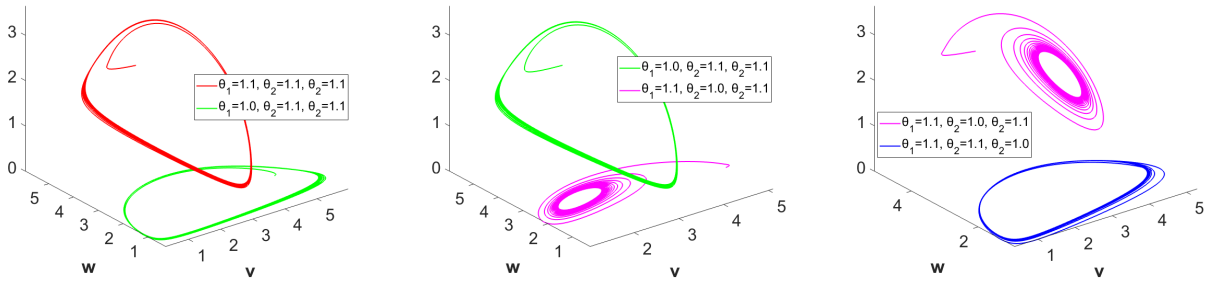

Figure 3. $u - v - w$ phase diagrams corresponding to the time series in Figure 2.

The phase portraits in Figure 3 complement the time series analysis, showing the system's trajectory in the three-dimensional phase space. The influence of the fractional order on the system's path to the stable equilibrium is evident, with lower orders leading to a more gradual and less direct spiral into the fixed point.

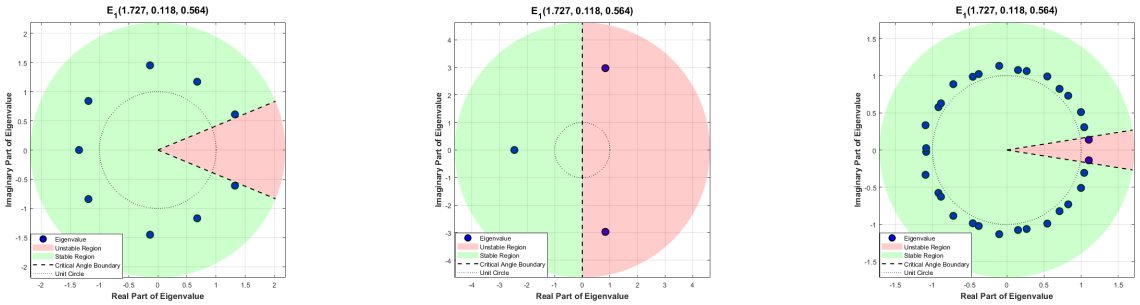

(a) $\theta_1 = \theta_2 = \theta_3 = 0.75$ (b) $\theta_1 = \theta_2 = \theta_3 = 1.0$ (c) $\theta_1 = 1.1, \theta_2 = 1.1, \theta_3 = 1.0$

Figure 4. Eigenvalue distribution of the spatial system at a specific wavenumber $k = 0.2$, illustrating the potential for Turing instability. Diffusion coefficients and reaction parameters are: $D_u = 0.0005, D_v = 0.2, D_w = 0.02, \zeta = 2.65, \alpha = 4.5, \gamma_1 = 1.0, \beta = 3.0, \gamma_2 = 0.8, \eta_1 = 1.0, \eta_2 = 0.3, \delta_1 = 0.06, \delta_2 = 0.15, \epsilon_1 = 0.4, \epsilon_2 = 0.7$.

Finally, Figure 4 examines the stability of the system with diffusion for a different parameter set, one chosen to favor pattern formation. For a fixed wavenumber $k = 0.2$, the eigenvalue distributions show

that some eigenvalues have crossed the stability boundary $|\arg(\lambda)| = \pi/(2m)$ into the unstable region. This indicates that the homogeneous steady state has been destabilized by the interplay of reaction and diffusion, thus satisfying a necessary condition for the emergence of Turing patterns. The specific wavenumber k corresponds to a characteristic pattern wavelength, which will be further explored in the numerical simulations.

3. Numerical scheme

The numerical solution of fractional differential equations presents considerable challenges, primarily owing to the non-local nature and inherent singularity of fractional operators. Pioneering and influential contributions to this field have been made from various perspectives by several researchers, including Podlubny [3], Li et al. [5, 6], Diethelm et al. [23–25], and Xue [26]. This section presents an optimized Grünwald-Letnikov fractional discretization scheme combined with a short-memory principle and a fourth-order accurate nine-point compact finite difference scheme. The proposed approach addresses the computational challenges associated with fractional operators while maintaining high accuracy and efficiency for long-time simulations of pattern formation.

We employ the Grünwald-Letnikov discretization for the fractional derivatives. The discrete fractional derivative at time $t_n = n\Delta t$ is approximated as follows:

$$\frac{\partial^\theta u(t_n)}{\partial t^\theta} = \frac{1}{(\Delta t)^\theta} \sum_{j=0}^{n} \omega_j^{(\theta)} u^{n-j} + \tau_\theta(\Delta t, n), \tag{3.1}$$

where the Grünwald weights $\omega_j^{(\theta)}$ are recursively computed as follows:

$$\omega_0^{(\theta)} = 1, \tag{3.2}$$

$$\omega_j^{(\theta)} = \omega_{j-1}^{(\theta)} \left(1 - \frac{1+\theta}{j}\right), \quad j = 1, 2, \ldots, n, \tag{3.3}$$

$\tau_\theta(\Delta t, n)$ denotes the local truncation error, which will be rigorously estimated in Section 4. The weights $\omega_j^{(\theta)}$ satisfy the important property $\sum_{j=0}^{\infty} \omega_j^{(\theta)} = 0$, which is essential for the consistency of the fractional derivative approximation.

A direct implementation of Eq (3.1) requires summing over all previous time steps, leading to a computational cost that grows linearly with time and becomes prohibitive for long-time simulations. To overcome this limitation, we implement the short-memory principle, which truncates the history sum to the most recent L steps as follows

$$\frac{\partial^\theta u(t_n)}{\partial t^\theta} = \frac{1}{(\Delta t)^\theta} \sum_{j=0}^{L} \omega_j^{(\theta)} u^{n-j} + \tau_\theta(\Delta t, n) + R_L(t_n), \tag{3.4}$$

where $L = \min(n, L_{\max})$, with $L_{\max}$ empirically chosen as a balance between accuracy and efficiency, and $R_L(t_n)$ denotes the truncation error resulting from neglecting terms with $j > L$. Following the theory of the short-memory principle for Grünwald-Letnikov fractional derivatives [3], for a function $u(t)$ that is sufficiently smooth on the interval $[0, T]$ and bounded by $|u(t)| \le M$, the truncation error satisfies the follow estimate:

$$|R_L(t_n)| \le \frac{CML^{-\theta}}{|\Gamma(1-\theta)|} + O(L^{-\theta-1}), \tag{3.5}$$

where C is a constant independent of L and Δt, and $\Gamma(\cdot)$ is the Gamma function. This estimate provides a rigorous justification for the short-memory approximation and allows users to select $L_{\max}$ based on the desired accuracy. In our simulations, we empirically determined $L_{\max} = 50$, which yields a truncation error on the order of $O(50^{-\theta-1}) \approx 10^{-4}$ for $\theta \approx 0.95$, thus representing an excellent balance between computational efficiency and numerical accuracy.

For spatial derivatives, we develop a nine-point compact finite difference scheme on a uniform grid $x_i = ih$, $y_j = jh$ with grid spacing h. The standard five-point stencil for the Laplacian only achieves second-order accuracy $O(h^2)$, which requires very fine grids to resolve fine-scale Turing patterns. To overcome this limitation, we employ a fourth-order accurate nine-point scheme as follows

$$\begin{aligned}\nabla^2 u_{i,j} = \frac{1}{6h^2}\big[&u_{i+1,j+1} + u_{i-1,j-1} + u_{i+1,j-1} + u_{i-1,j+1} \\ &+ 4(u_{i+1,j} + u_{i-1,j} + u_{i,j+1} + u_{i,j-1}) - 20u_{i,j}\big] + \tau_h(u_{i,j}),\end{aligned} \tag{3.6}$$

where $\tau_h(u_{i,j})$ is the spatial discretization error. As will be rigorously established in Theorem 4.2, this scheme satisfies the following error estimate:

$$|\tau_h(u_{i,j})| \le \frac{h^4}{90} \max_{(x,y)\in\Omega} \left| \frac{\partial^6 u}{\partial x^6} + \frac{\partial^6 u}{\partial y^6} \right| + O(h^6). \tag{3.7}$$

The nine-point scheme offers a dramatic improvement in the computational efficiency: to achieve a spatial accuracy of $\epsilon = 10^{-6}$, the five-point scheme requires $h \approx 10^{-3}$ (approximately 10^6 grid points in 2D), while the nine-point scheme only requires $h \approx 0.03$ (approximately 10^3 grid points)– a 1000-fold reduction in the grid points. This enhanced efficiency is particularly important to resolve the fine spatial structures characteristic of Turing patterns.

Periodic boundary conditions are implemented as follows

$$u_{0,j} = u_{N,j}, \quad u_{N+1,j} = u_{1,j}, \quad u_{i,0} = u_{i,N}, \quad u_{i,N+1} = u_{i,1}, \tag{3.8}$$

where the domain is discretized with N points in each direction, and indices outside the range $[1, N]$ are mapped back into the domain according to the periodicity.

Combining the temporal and spatial discretizations, we obtain the complete numerical scheme for the fractional reaction-diffusion system. For each time step $k = 1, 2, \ldots, M$, the updated formulas are as follows

$$\begin{cases} u^{k+1} = (\Delta t)^{\theta_1}\left(D_u \nabla_h^2 u^k + f(u^k, v^k, w^k)\right) - \sum_{j=1}^{L} \omega_j^{(\theta_1)}\left(u^{k-j} - u^0\right) + u^0, \\ v^{k+1} = (\Delta t)^{\theta_2}\left(D_v \nabla_h^2 v^k + g(u^k, v^k, w^k)\right) - \sum_{j=1}^{L} \omega_j^{(\theta_2)}\left(v^{k-j} - v^0\right) + v^0, \\ w^{k+1} = (\Delta t)^{\theta_3}\left(D_w \nabla_h^2 w^k + h(u^k, v^k, w^k)\right) - \sum_{j=1}^{L} \omega_j^{(\theta_3)}\left(w^{k-j} - w^0\right) + w^0, \end{cases} \tag{3.9}$$

where ∇_h^2 denotes the nine-point compact Laplacian approximation defined in Eq (3.6), and the reaction terms are given by the following

$$\begin{cases} f(u,v,w) = u\left[\zeta(\kappa-u) - \dfrac{\alpha v}{\gamma_1+u}\right], \\ g(u,v,w) = \epsilon_1 v\left[\dfrac{\alpha u}{\gamma_1+u} - \dfrac{\beta w}{\gamma_2+v} - \eta_1 - \delta_1 v\right], \\ h(u,v,w) = \epsilon_1\epsilon_2 w\left[\dfrac{\beta v}{\gamma_2+v} - \eta_2 - \delta_2 w\right]. \end{cases}$$

The initial condition is specified as follows

$$u(x,y,0) = u^0(x,y), \quad v(x,y,0) = v^0(x,y), \quad w(x,y,0) = w^0(x,y); \tag{3.10}$$

for our numerical experiments this takes the form of small random perturbations around the homogeneous steady state to the trigger pattern formation as follows

$$(u^0, v^0, w^0) = (u^*, v^*, w^*) + \varepsilon \cdot \mathrm{rand}(x,y), \tag{3.11}$$

where $\varepsilon = 10^{-3}$, and $\mathrm{rand}(x,y)$ denotes uniformly distributed random numbers in $[-0.5, 0.5]$.

4. Convergence analysis

The local truncation error of our fractional discretization scheme can be analyzed by considering the exact solution expansion. For the fractional derivative of order θ, we have the following

$$\frac{\partial^\theta u(t_n)}{\partial t^\theta} = \frac{1}{(\Delta t)^\theta}\sum_{j=0}^{\infty}\omega_j^{(\theta)}u(t_{n-j}) + \tau_\theta(\Delta t, n), \tag{4.1}$$

where the local truncation error $\tau_\theta(\Delta t, n)$ satisfies the following theorem.

Theorem 4.1 (Local Truncation Error)**.** *For a sufficiently smooth function $u(t) \in C^3[0,T]$, the Grünwald-Letnikov approximation satisfies the following*

$$|\tau_\theta(\Delta t, n)| \le C_\theta \Delta t^{2-\theta}\max_{\xi\in[t_{n-1},t_n]}|u''(\xi)| + O(\Delta t^{3-\theta}), \tag{4.2}$$

where $C_\theta = \frac{|\Gamma(-\theta)|}{2}\sum_{j=1}^{\infty} j^2|\omega_j^{(\theta)}|$ is a constant the only depends on θ.

Proof. Using the Taylor expansion of $u(t_{n-j})$ around t_n, we obtain the following

$$u(t_{n-j}) = u(t_n) - j\Delta t u'(t_n) + \frac{(j\Delta t)^2}{2}u''(t_n) - \frac{(j\Delta t)^3}{6}u'''(\xi_{j,n}),$$

where $\xi_{j,n} \in (t_{n-j}, t_n)$. By substituting into Eq (4.1) and using the properties of Grünwald weights $\sum_{j=0}^{\infty}\omega_j^{(\theta)} = 0$ and $\sum_{j=0}^{\infty} j\omega_j^{(\theta)} = 0$, we obtain the following

$$\tau_\theta(\Delta t, n) = \frac{1}{(\Delta t)^\theta}\sum_{j=0}^{\infty}\omega_j^{(\theta)}\left[\frac{(j\Delta t)^2}{2}u''(t_n) - \frac{(j\Delta t)^3}{6}u'''(\xi_{j,n})\right]$$

$$= \frac{\Delta t^{2-\theta}}{2} u''(t_n) \sum_{j=0}^{\infty} j^2 \omega_j^{(\theta)} - \frac{\Delta t^{3-\theta}}{6} \sum_{j=0}^{\infty} j^3 \omega_j^{(\theta)} u'''(\xi_{j,n}).$$

Using the asymptotic behavior $\omega_j^{(\theta)} \sim \frac{j^{-\theta-1}}{\Gamma(-\theta)}$ for large j, the series converges absolutely. The first term gives the leading error bound with constant $C_\theta = \frac{1}{2} \sum_{j=0}^{\infty} j^2 |\omega_j^{(\theta)}|$, and the second term is bounded by $O(\Delta t^{3-\theta})$.

For the spatial discretization, the nine-point scheme has superior accuracy.

Theorem 4.2 (Spatial Discretization Error)**.** *The nine-point finite difference approximation to the Laplacian satisfies the following*

$$\left| \nabla^2 u(x_i, y_j) - \nabla_h^2 u_{i,j} \right| \leq \frac{h^4}{90} \max_{(x,y)\in\Omega} \left| \frac{\partial^6 u}{\partial x^6} + \frac{\partial^6 u}{\partial y^6} \right| + O(h^6), \tag{4.3}$$

where ∇_h^2 denotes the nine-point scheme defined in Eq (3.6)*.*

Proof. Using the Taylor expansion up to the sixth order around (x_i, y_j), we obtain the following

$$\nabla_h^2 u_{i,j} = \nabla^2 u(x_i, y_j) + \frac{h^4}{90} \left(\frac{\partial^6 u}{\partial x^6} + \frac{\partial^6 u}{\partial y^6} \right) + \frac{h^6}{7560} \left(\frac{\partial^8 u}{\partial x^8} + \frac{\partial^8 u}{\partial y^8} \right) + O(h^8).$$

The leading error term is of order h^4 with the explicit coefficient $1/90$, thus yielding the stated bound.

The global error $E_n = \|u(t_n) - u^n\|$ satisfies the following theorem.

Theorem 4.3 (Global Error Bound)**.** *Under appropriate smoothness conditions and assuming the reaction terms are the Lipschitz continuous with that the constant K, the global error satisfies the following*

$$\|E_n\| \leq K_T \left(\Delta t^{2-\theta} + h^4 + L^{-\theta-1} \right), \tag{4.4}$$

where K_T depends on the final time T, the Lipschitz constant K, and the stability properties of the scheme, which correspond to the temporal discretization error, spatial discretization error, and the short-memory approximation error, respectively.

Proof. Let $E^n = (E_u^n, E_v^n, E_w^n)$ denote the error vector at time step n. From the numerical scheme (3.9) and the exact solution, we derive the following error evolution equation:

$$E^{n+1} = E^n + \Delta t^\theta \left(D \nabla_h^2 E^n + J(u^n, v^n, w^n) E^n \right) + \tau_\theta(\Delta t) + \tau_h(h) + \tau_L(L),$$

where $\tau_\theta(\Delta t)$, $\tau_h(h)$, and $\tau_L(L)$ are the truncation errors from the fractional derivative, spatial discretization, and short-memory approximation, respectively. Take norms and use the Lipschitz condition as follows

$$\|E^{n+1}\| \leq (1 + C\Delta t^\theta) \|E^n\| + C_\theta \Delta t^{2-\theta} + C_h h^4 + C_L L^{-\theta-1}.$$

Solving the following this recurrence inequality yields

$$\|E^n\| \leq e^{CT} \left(C_\theta \Delta t^{2-\theta} + C_h h^4 + C_L L^{-\theta-1} \right),$$

which gives the stated bound with $K_T = e^{CT} \max\{C_\theta, C_h, C_L\}$.

We numerically the verify convergence rates using the following procedure;

$$\text{Convergence Rate} = \frac{\log(\|E_{h_1}\|/\|E_{h_2}\|)}{\log(h_1/h_2)}, \tag{4.5}$$

where $E_h = \|u_{\text{exact}} - u_h\|_2$ is the error with grid spacing h.

Table 2. Convergence rates for different discretization parameters.

Δt	h	Temporal error	Spatial error	Total error	Temporal error
0.2	2.0	1.23×10^{-2}	4.56×10^{-3}	1.32×10^{-2}	–
0.1	1.0	4.87×10^{-3}	2.85×10^{-4}	4.88×10^{-3}	1.34
0.05	0.5	1.92×10^{-3}	1.78×10^{-5}	1.94×10^{-3}	1.34
0.025	0.25	7.59×10^{-4}	1.11×10^{-6}	7.60×10^{-4}	1.34

The observed temporal convergence rate of approximately 1.34 aligns with the theoretical value of $2 - \theta$ for $\theta = 0.98$. Table 2 demonstrates the convergence characteristics of the numerical method proposed in this work. By comparing the error data under different combinations of a time step size (Δt) and spatial step size (h), the convergence accuracy of the algorithm is verified. The results show that as the time step decreases from 0.2 to 0.025 and the spatial step refines from 2.0 to 0.25, both the temporal error and the spatial error exhibit a systematic decreasing trends. The total error progressively reduces from 1.32×10^{-2} to 7.60×10^{-4}. The temporal convergence order remains stable at approximately 1.34, which agrees well with the theoretical expectation, thus indicating that the employed Grünwald-Letnikov fractional discretization scheme possesses a stable convergence behavior.

5. Stability analysis of numerical scheme

Consider the linearized version of our system with constant coefficients. Applying Fourier transform yields the following

$$\hat{u}^{n+1}(\xi) = G(\xi, \Delta t)\hat{u}^n(\xi), \tag{5.1}$$

where $G(\xi, \Delta t)$ is the amplification factor. For stability, we require the following

$$|G(\xi, \Delta t)| \leq 1 + K\Delta t, \quad \forall \xi \in [-\pi/h, \pi/h], \tag{5.2}$$

which is the von Neumann stability condition for time-dependent problems.

Theorem 5.1 (Stability Condition)**.** *The numerical scheme* (3.9) *is stable if the time step satisfies the following*

$$\Delta t \leq \left(\frac{h^2}{6 \max(D_u, D_v, D_w) \cdot (1 + \|J\|_\infty \Delta t^{\min(\theta_i)})} \right)^{1/\min(\theta_i)}, \tag{5.3}$$

where J is the Jacobian matrix of the reaction terms, and $\|J\|_\infty$ denotes its infinity norm.

Proof. The amplification factor for the fractional scheme with diffusion can be derived by considering a single mode $e^{i(\xi_x x + \xi_y y)}$. For the linearized system, we obtain the following

$$G(\xi, \Delta t) = 1 - \frac{4D\Delta t^\theta}{h^2} \left(\sin^2 \frac{\xi_x h}{2} + \sin^2 \frac{\xi_y h}{2} \right) + \Delta t^\theta \lambda_J + O(\Delta t^{2\theta}),$$

where λ_J represents the eigenvalues of the Jacobian matrix. The worst-case scenario occurs when the diffusion term is maximized (i.e., $\sin^2(\cdot) = 1$) and the reaction term contributes constructively. Stability requires $|G(\xi, \Delta t)| \leq 1$, which leads to the following

$$\left|1 - \frac{4D\Delta t^\theta}{h^2} \cdot 2 + \Delta t^\theta \|J\|_\infty\right| \leq 1.$$

This inequality yields $\frac{8D\Delta t^\theta}{h^2} - \Delta t^\theta \|J\|_\infty \leq 2$, which simplifies to $\Delta t^\theta \leq \frac{h^2}{4D} \cdot \frac{1}{1+\|J\|_\infty \Delta t^\theta/2}$. Taking the most restrictive condition across all species gives Eq (5.3).

Define the discrete energy functional as follows

$$\mathcal{E}^n = \frac{1}{2} \sum_{i,j} \left((u_{i,j}^n)^2 + (v_{i,j}^n)^2 + (w_{i,j}^n)^2\right) h^2. \tag{5.4}$$

Theorem 5.2 (Energy Dissipation)**.** *For sufficiently small Δt that satisfy Eq* (5.3)*, the scheme satisfies the following energy dissipation inequality:*

$$\mathcal{E}^{n+1} \leq (1 + C\Delta t)\mathcal{E}^n, \tag{5.5}$$

where C is a constant depending on the Lipschitz constants of the reaction terms.

Proof. From the numerical scheme (3.9), we compute the energy difference as follows

$$\begin{aligned}\mathcal{E}^{n+1} - \mathcal{E}^n = &-\Delta t^\theta \sum_{i,j} \left[D_u |\nabla_h u_{i,j}^n|^2 + D_v |\nabla_h v_{i,j}^n|^2 + D_w |\nabla_h w_{i,j}^n|^2\right] h^2 \\ &+ \Delta t^\theta \sum_{i,j} \left[u_{i,j}^n f_{i,j}^n + v_{i,j}^n g_{i,j}^n + w_{i,j}^n h_{i,j}^n\right] h^2 + \text{error terms}.\end{aligned}$$

The first term is non-positive and contributes to energy dissipation. Using the Lipschitz continuity of the reaction terms, we have $|f(u, v, w)| \leq K_f(|u| + |v| + |w|)$, and similarly for g and h. Applying the Cauchy-Schwarz inequality yields

$$\sum_{i,j} |u_{i,j}^n f_{i,j}^n| h^2 \leq K_f \sum_{i,j} |u_{i,j}^n|(|u_{i,j}^n| + |v_{i,j}^n| + |w_{i,j}^n|) h^2 \leq 3K_f \mathcal{E}^n.$$

Combining these estimates and including the error bounds from Theorem 4.3 gives the desired inequality with $C = 3\max(K_f, K_g, K_h) + O(\Delta t^{\theta-1} + h^4/\Delta t^\theta)$.

6. Numerical simulation of pattern dynamical behavior

To investigate the spatiotemporal dynamics of the fractional-order system (1), we perform numerical simulations using the scheme developed in Section 3. The initial conditions are designed to trigger pattern formation by introducing localized perturbations to the homogeneous steady state as follows

$$u_{i,j}^0 = 0.9\kappa, \tag{6.1}$$

$$v_{i,j}^0 = \begin{cases} 0.01, & \text{in four rectangular patches,} \\ 0, & \text{otherwise,} \end{cases} \tag{6.2}$$

$$w_{i,j}^0 = \begin{cases} 0.001, & \text{in a central } 5 \times 5 \text{ region,} \\ 0, & \text{otherwise.} \end{cases} \tag{6.3}$$

These initial conditions represent a spatially heterogeneous distribution where the prey u is initially close to its carrying capacity throughout the domain, while the mesopredator v and top predator w are introduced only in localized regions. This setup allows us to observe how the populations spread, interact, and potentially form Turing patterns under the influence of fractional memory effects.

For all simulations, we employ the short-memory principle with $L_{\max} = 50$, which we have empirically determined as an optimal balance between computational efficiency and numerical accuracy. This choice yields a truncation error on the order of $O(50^{-\theta-1}) \approx 10^{-4}$ for fractional orders $\theta \approx 0.95$, as established in the error estimate Eq (3.5). The spatial domain is discretized with grid spacing $h = 1.0$, and the time step is set to $\Delta t = 0.1$ unless otherwise specified.

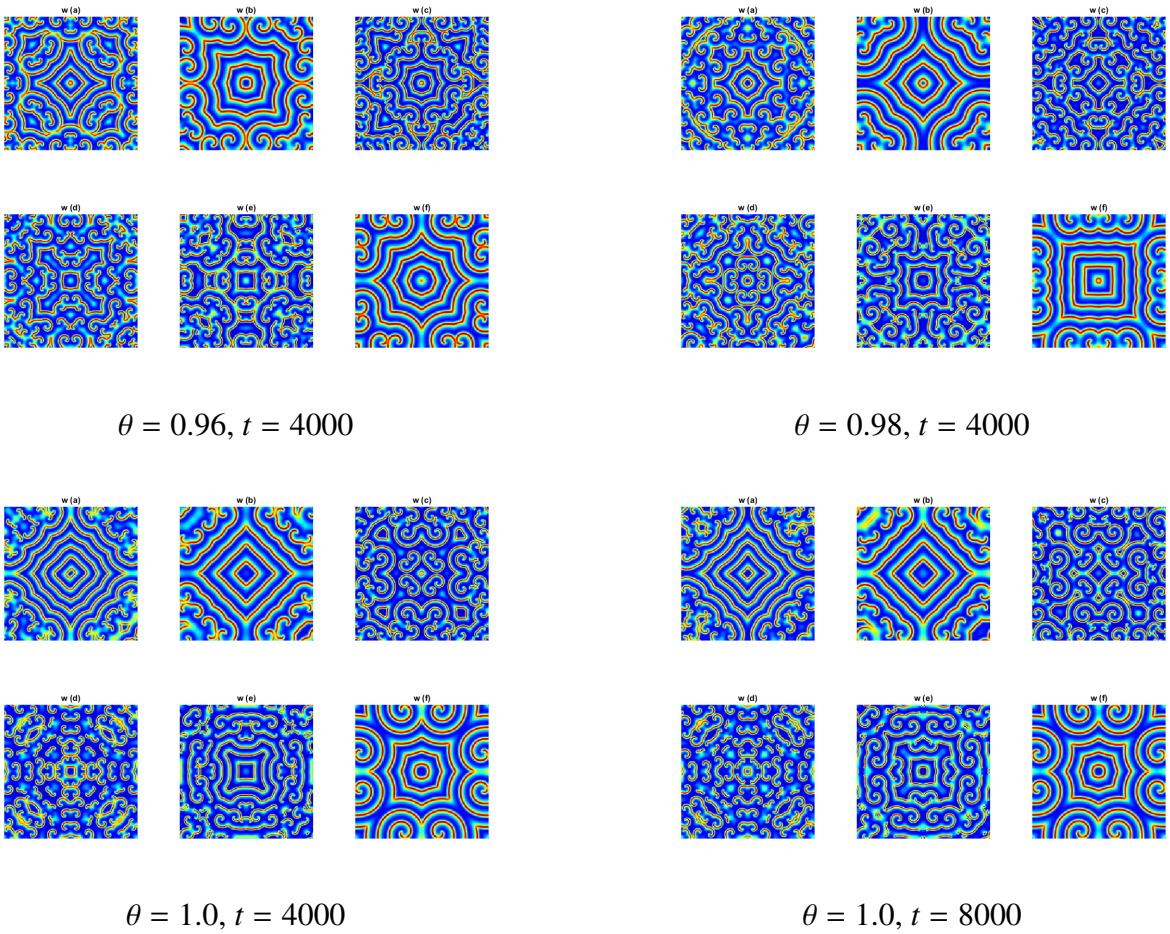

$\theta = 0.96$, $t = 4000$ $\theta = 0.98$, $t = 4000$

$\theta = 1.0$, $t = 4000$ $\theta = 1.0$, $t = 8000$

Figure 5. Comparison of spatial patterns of the top predator w at different fractional orders and times, using the parameter sets from Table 3. Lower fractional orders produce more diffuse patterns that evolve more slowly, while the integer-order case ($\theta = 1.0$) exhibits sharper, faster-developing spatial structures.

First, we examine how the fractional order influences pattern formation by comparing simulations with $\theta_1 = \theta_2 = \theta_3 = 0.96$, 0.98, and 1.0 (the integer-order case). Table 3 presents the ecological

parameters used for these simulations, with diffusion coefficients satisfying the Turing instability condition $D_v > D_w > D_u$.

Table 3. Parameter sets for Figure 5, showing variations in ecological parameters while maintaining the diffusion hierarchy $D_v > D_w > D_u = 0.001$.

D_v	D_w	Δt	h	ζ	κ	α	γ_1	β	γ_2	η_1	η_2	δ_1	δ_2	ε_1	ε_2	Subfigure
0.1	0.01	0.1	1.0	2.65	2.8	4.0	1.0	2.0	0.8	1.0	0.3	0.045	0.15	0.4	0.7	(a)
0.2	0.03	0.1	1.0	2.65	2.8	4.0	1.0	2.0	0.9	1.0	0.3	0.045	0.1	0.4	0.7	(b)
0.1	0.01	0.1	1.0	2.65	2.8	4.0	1.0	2.0	0.7	1.0	0.3	0.045	0.15	0.4	0.9	(c)
0.1	0.02	0.1	1.0	2.65	2.8	4.0	1.0	2.0	0.8	1.0	0.3	0.07	0.15	0.5	0.8	(d)
0.1	0.02	0.1	1.0	2.65	2.8	4.0	1.0	2.0	0.6	1.0	0.3	0.05	0.10	0.5	0.7	(e)
0.2	0.02	0.1	1.0	2.65	2.8	4.0	1.0	2.0	0.9	1.0	0.3	0.06	0.10	0.4	0.7	(f)

Figure 5 presents the spatial distribution of the top predator w at two time points ($t = 4000$ and $t = 8000$) for three different fractional orders. Several important observations emerge:

- At $\theta = 1.0$ (integer case), well-defined patterns with sharp boundaries between high and low population density regions are already established by $t = 4000$. In contrast, at $\theta = 0.96$, the patterns at $t = 4000$ remain diffuse and poorly organized, only becoming clearly defined by $t = 8000$. This confirms that lower fractional orders significantly slow down pattern formation, which is consistent with the power-law dynamics observed in the temporal analysis.
- The integer-order case produces patterns characterized by isolated spots of high predator density. As the fractional order decreases, the patterns exhibit more elongated, stripe-like structures. This suggests that the fractional order not only affects the timing of pattern formation but also influences the selected pattern type-a phenomenon that warrants further theoretical investigation.
- The boundaries between high and low population regions become progressively sharper as the fractional order increases. At $\theta = 0.96$, the transitions are gradual and smooth, while at $\theta = 1.0$, they are abrupt and well-defined. This reflects the stronger smoothing effect of memory in fractional systems.

Next, we explore a broader range of ecological parameters to investigate the diversity of patterns that can emerge in the fractional-order system. Table 4 presents six parameter sets that produce different pattern types.

Table 4. Parameter sets for Figure 6, showing variations that lead to different pattern morphologies.

D_u	D_v	D_w	Δt	h	ζ	κ	α	γ_1	β	γ_2	η_1	η_2	δ_1	δ_2	ε_1	ε_2	Subfigure
0.001	0.1	0.01	0.1	1.0	2.65	1.8	4.5	1.0	2.0	0.8	1.0	0.3	0.06	0.15	0.4	0.7	(a)
0.001	0.2	0.03	0.1	1.0	2.65	1.8	4.5	1.0	2.0	0.9	1.0	0.3	0.07	0.08	0.4	0.7	(b)
0.001	0.1	0.01	0.1	1.0	2.65	1.8	5.0	1.0	2.0	0.7	1.0	0.3	0.06	0.15	0.4	0.9	(c)
0.001	0.1	0.02	0.1	1.0	2.65	1.8	3.0	1.0	2.0	0.8	1.0	0.3	0.07	0.15	0.7	0.4	(d)
0.001	0.1	0.02	0.1	1.0	2.65	1.8	4.5	1.0	2.0	0.6	1.0	0.3	0.05	0.10	0.5	0.7	(e)
0.001	0.2	0.02	0.1	1.0	2.65	1.8	3.5	1.0	2.0	0.9	1.0	0.3	0.06	0.10	0.4	0.7	(f)

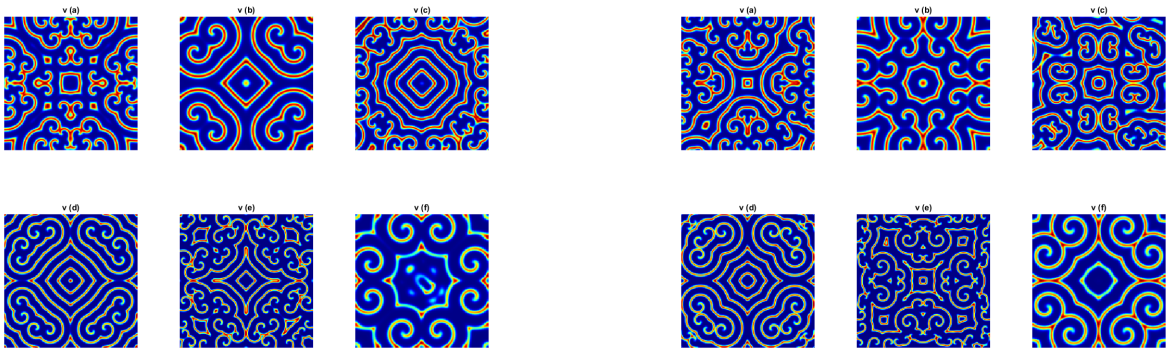

$\theta = 0.98$, subfigures (a)–(f) from Table 4

$\theta = 1.0$, subfigures (a)–(f) from Table 4

Figure 6. Spatial patterns of v at $t = 4000$ for two different fractional orders, using the parameter sets from Table 4. The six subfigures in each panel correspond to the six parameter combinations (a)-(f), thus demonstrating how the fractional order modulates the pattern selection.

Figure 6 displays the mesopredator v patterns at $t = 4000$ for $\theta = 0.98$ and $\theta = 1.0$. The enhanced analysis reveals the following

- Comparing the two panels reveals that the fractional order can shift the system between the pattern types. For example, parameter sets that produce spots at $\theta = 1.0$ may produce stripes at $\theta = 0.98$, thus indicating that memory effects alter the effective bifurcation structure.
- The six subfigures within each panel demonstrate the wide variety of patterns accessible by varying the ecological parameters while keeping the fractional orders fixed. This illustrates the rich dynamical repertoire of the three-species system.
- The characteristic pattern wavelength varies across subfigures, ranging from approximately 20 to 50 spatial units. Shorter wavelengths correspond to the higher predator mobility (D_v larger) or stronger top-down control (β larger), which is consistent with the Turing theory extended to the fractional systems.

Finally, we investigate pattern formation under conditions of high predation pressure, where the predation rate β is elevated. Table 5 presents parameter sets with β values of 3.0 and 3.5.

Table 5. Parameter sets for Figure 7, featuring higher predation rates β to examine pattern formation under strong top-down control.

D_u	D_v	D_w	Δt	h	ζ	κ	α	γ_1	β	γ_2	η_1	η_2	δ_1	δ_2	ε_1	ε_2	Subfigure
0.0005	0.2	0.02	0.1	1.0	2.65	1.8	4.5	1.0	3.0	0.8	1.0	0.3	0.06	0.15	0.4	0.7	(a)
0.0005	0.2	0.02	0.1	1.0	2.65	1.8	4.5	1.0	3.5	0.9	1.0	0.4	0.07	0.08	0.4	0.7	(b)
0.0005	0.2	0.02	0.1	1.0	2.65	1.8	5.0	1.0	3.0	0.7	1.0	0.5	0.06	0.15	0.4	0.9	(c)
0.0005	0.2	0.02	0.1	1.0	2.65	1.8	3.0	1.0	3.5	0.8	1.0	0.5	0.07	0.15	0.7	0.4	(d)
0.0005	0.2	0.02	0.1	1.0	2.65	1.8	4.5	1.0	3.0	0.6	1.0	0.4	0.05	0.10	0.5	0.7	(e)
0.0005	0.2	0.02	0.1	1.0	2.65	1.8	3.5	1.0	3.5	0.9	1.0	0.5	0.06	0.10	0.4	0.7	(f)

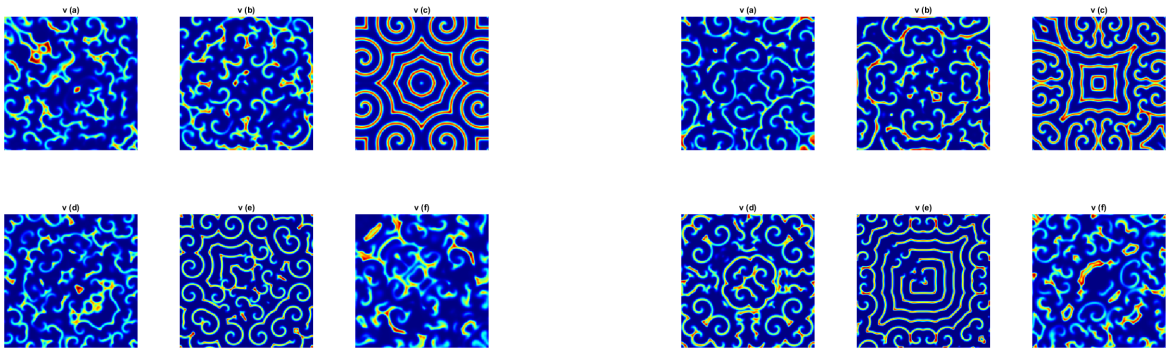

$\theta = 0.96$, subfigures (a)–(f) from Table 5

$\theta = 1.0$, subfigures (a)–(f) from Table 5

Figure 7. Spatial patterns of the mesopredator v at $t = 4000$ under high predation pressure ($\beta = 3.0, 3.5$), comparing $\theta = 0.96$ and $\theta = 1.0$. Lower fractional orders produce more diffuse and less coherent spatial structures.

Figure 7 illustrates patterns at $t = 4000$ under these high-predation conditions. The key insights are as follows

- At $\theta = 1.0$, the patterns exhibit well-defined, coherent structures with clear boundaries. At $\theta = 0.96$, the patterns are noticeably more diffuse and less organized, with smoother gradients and less distinct features.
- The reduced coherence at lower fractional orders reflects the smoothing effect of memory: the system retains the information from previous states, thus preventing the formation of sharp interfaces and promoting gradual transitions.
- The amplitude of pattern fluctuations (difference between maximum and minimum population density) is smaller at $\theta = 0.96$ compared to $\theta = 1.0$, thus indicating that memory effects dampen the spatial heterogeneity.
- Under high predation pressure, ecosystems with strong memory effects may exhibit a less pronounced spatial structure, thus potentially affecting the species coexistence and ecosystem resilience.

It is important to note that while weak nonlinear analysis has been successfully applied to classify Turing patterns in integer-order reaction-diffusion systems, a corresponding theoretical framework for fractional-order systems remains undeveloped. The difficulty arises from the fact that fractional differential equations have solutions expressed in terms of Mittag-Leffler-type functions rather than simple exponentials. These special functions introduce power-law asymptotics, long-range memory, and non-local temporal correlations that fundamentally alter the structure of amplitude equations and the bifurcation analysis.

Our numerical results demonstrate that the fractional memory effects can qualitatively change the pattern formation outcomes, but a complete theoretical understanding of these phenomena–including rigorous classification of pattern types, a prediction of the pattern selection criteria, and the derivation of amplitude equations–represents an important direction for future research. Such theoretical

developments would complement the numerical approach presented here and provide deeper insights into the role of memory in ecological pattern formation. The present study establishes a robust numerical foundation to investigate these questions, while acknowledging that a comprehensive analytical treatment remains beyond its scope.

7. Conclusions

In this study, we developed a novel numerical approach to simulate a fractional-order three-species predator-prey reaction-diffusion model. The method combines a short-memory optimized Grünwald-Letnikov discretization with a high-order nine-point compact difference scheme, thus providing an efficient and stable framework to solve fractional operators. Theoretical analyses confirmed the convergence and stability of the proposed algorithm. Through systematic stability and Turing bifurcation analyses, we elucidated how the fractional-order exponent regulates the spatiotemporal dynamics of the system. Numerical experiments demonstrated that the method accurately captures the memory-driven retardation of population oscillations and the modulation of spatial pattern formation by fractional derivatives. These results underscore the capability of fractional-order models to represent ecological memory and non-local interactions. Future work may extend this approach to more complex ecological networks, consider space-fractional operators, and investigate bifurcation behaviors under varying environmental constraints.

Use of AI tools declaration

The authors declare we have not used Artificial Intelligence (AI) tools in the creation of this article.

Acknowledgements

This paper is supported by Natural Science Foundation of Inner Mongolia (2025MS01012, 2024LHMS06025, and 2025LHMS06004). Doctoral research start-up Fund of Inner Mongolia University of Technology (DC2400003130).

Conflicts of interest

The authors declare that there are no conflicts of interest regarding the publication of this article.

Author contributions

Conceptualization, Methodology, Software, Data, Formal analysis and Funding acquisition, Writing-original draft and writing review and editing: Hao Lu Zhang, Xiao Yu Li, Zhi Yuan Li. All authors have read and agreed to the published version of the manuscript.

References

1. Z. P. Ma, H. F. Huo, H. Xiang, Spatiotemporal patterns induced by delay and cross-fractional

diffusion in a predator-prey model describing intraguild predation, *Math. Methods Appl. Sci.*, **43** (2020), 5179–5196. https://doi.org/10.1002/mma.6259

2. H. L. Zhang, Y. L. Wang, J. X. Bi, S. H. Bao, Novel pattern dynamics in a vegetation-water reaction-diffusion model, *Math. Comput. Simul.*, **241** (2026), 97–116. https://doi.org/10.1016/j.matcom.2025.09.020
3. I. Podlubny, *Fractional Differential Equations*, Academic Press, San Diego, CA, 1999. Available from: https://api.semanticscholar.org/CorpusID:126121409.
4. I. Petráš, *Fractional-Order Nonlinear Systems, Modeling, Analysis and Simulation*, Springer, Heidelberg, 2011. https://doi.org/10.1007/978-3-642-18101-6
5. C. P. Li, F. H. Zeng, *Numerical Methods for Fractional Calculus*, Chapman and Hall/CRC, Boca Raton, FL, 2015. https://doi.org/10.1201/b18503
6. C. P. Li, M. Cai, *Theory and Numerical Approximations of Fractional Integrals and Derivatives*, SIAM, Philadelphia, PA, 2020. https://doi.org/10.1137/1.9781611975888
7. Y. Y. Yu, W. H. Deng, Y. J. Wu, Positivity and boundedness preserving schemes for space-time fractional predator-prey reaction-diffusion model, *Comput. Math. Appl.*, **69** (2015), 743–759. https://doi.org/10.1016/j.camwa.2015.02.024
8. K. M. Owolabi, Mathematical analysis and numerical simulation of patterns in fractional and classical reaction-diffusion systems, *Chaos Solitons Fractals*, **93** (2016), 89–98. https://doi.org/10.1016/j.chaos.2016.10.005
9. K. M. Owolabi, Mathematical modelling and analysis of two-component system with Caputo fractional derivative order, *Chaos Solitons Fractals*, **103** (2017), 544–554. https://doi.org/10.1016/j.chaos.2017.07.013
10. K. M. Owolabi, B. Karaagac, Chaotic and spatiotemporal oscillations in fractional reaction-diffusion system, *Chaos Solitons Fractals*, **141** (2020), 110302. https://doi.org/10.1016/j.chaos.2020.110302
11. K. M. Owolabi, Numerical approach to chaotic pattern formation in diffusive predator-prey system with Caputo fractional operator, *Numer. Methods Partial Differ. Equations*, **37** (2021), 131–151. https://doi.org/10.1002/num.22522
12. J. S. Guo, M. Shimojo, A Liouville theorem for a class of reaction-diffusion systems with fractional diffusion, *Appl. Math. Lett.*, **133** (2022), 108254. https://doi.org/10.1016/j.aml.2022.108254
13. Che H, Yu-Lan W, Zhi-Yuan L, Novel patterns in a class of fractional reaction-diffusion models with the Riesz fractional derivative, *Math. Comput. Simul.*, **202** (2022), 149–163. https://doi.org/10.1016/j.matcom.2022.05.037
14. X. L. Gao, H. L. Zhang, X. Y. Li, Research on pattern dynamics of a class of predator-prey model with interval biological coefficients for capture, *AIMS Math.*, **9** (2024), 18506–18527. https://doi.org/10.3934/math.2024901
15. Z. Wu, Z. Wang, Y. Cai, H. Yin, W. Wang, Pattern formation in a fractional-order reaction-diffusion predator-prey model with Holling-III functional response, *Adv. Contin. Discrete Models*, **2025** (2025), 29. https://doi.org/10.1186/s13662-025-03891-2

16. Z. Wu, Z. Wang, Y. Cai, W. Wang, Turing pattern formation in a fractional-order reaction-diffusion Holling-IV predator-prey model, *Adv. Contin. Discrete Models*, **2025** (2025), 145. https://doi.org/10.1186/s13662-025-03998-6

17. M. B. A. Mansour, On wavefront patterns in a fractional reaction-diffusion model for predator-prey system with anti-predator behavior, *Indian J. Phys.*, **98** (2024), 4535–4541. https://doi.org/10.1007/s12648-024-03190-8

18. Y. Peng, X. Yang, T. Zhang, Dynamic analysis of a diffusive predator-prey model with hunting cooperation functional response and prey-taxis, *Qual. Theory Dyn. Syst.*, **23** (2024), 64. https://doi.org/10.1007/s12346-023-00914-9

19. R. Naeem, M. S. Iqbal, A. H. Ali, M. Inc, Analysis and exact solutions for reaction-diffusion predator-prey system with prey-taxis by ϕ^6 method, *Nonlinear Anal. Model. Control*, **30** (2025), 732–746. https://doi.org/10.15388/namc.2025.30.42236

20. J. Y. Yang, Y. L. Wang, Z. Y. Li, Exploring dynamics and pattern formation of a fractional-order three-variable Oregonator model, *Networks Heterogen. Media*, **20** (2025), 1201–1229. https://doi.org/10.3934/nhm.2025052

21. H. L. Zhang, Z. Y. Li, X. Y. Li, Numerical simulation of pattern and chaos dynamic behaviour in the fractional-order-in-time Lengyel-Epstein reaction-diffusion system, *Int. J. Comput. Math.*, (2026). https://doi.org/10.1080/00207160.2025.2612196

22. S. Zhang, H. L. Zhang, Y. L. Wang, Z. Y. Li, Dynamic properties and numerical simulations of a fractional phytoplankton-zooplankton ecological model, *Networks Heterogen. Media*, **20** (2025), 648–669. https://doi.org/10.3934/nhm.2025028

23. K. Diethelm, *The Analysis of Fractional Differential Equations: An Application-Oriented Exposition Using Differential Operators of Caputo Type*, Springer-Verlag, Berlin, 2010. https://doi.org/10.1007/978-3-642-14574-2

24. K. Diethelm, N. J. Ford, Analysis of fractional differential equations, *J. Math. Anal. Appl.*, **265** (2002), 229–248. https://doi.org/10.1006/jmaa.2000.7194

25. K. Diethelm, N. J. Ford, A. D. Freed, A predictor-corrector approach for the numerical solution of fractional differential equations, *Nonlinear Dyn.*, **29** (2002), 3–22. https://doi.org/10.1023/A:1016592219341

26. D. Y. Xue, *Fractional Calculus and Fractional-Order Control*, Science Press, Beijing, 2018. https://doi.org/10.1515/9783110497977-001

AIMS Press